High-Performance Phase Locking of Wide Linewidth Semiconductor Lasers by Combined Use of Optical Injection Locking and Optical Phase-Lock Loop

A. C. Bordonalli, C. Walton, and Alwyn J. Seeds, *Fellow, IEEE*

***Abstract*— The requirement for narrow linewidth lasers or short-loop propagation delay makes the realization of optical phase-lock loops using semiconductor lasers difficult. Although optical injection locking can provide low phase error variance for wide linewidth lasers, the locking range is restricted by stability considerations. Theoretical and experimental results for a system which combines both techniques so as to overcome these limitations, the optical injection phase-lock loop (OIPLL), are reported. Phase error variance values as low as 0.006 rad^2 (500 MHz bandwidth) and locking ranges exceeding 26 GHz were achieved in homodyne OIPLL systems using DFB lasers of summed linewidth 36 MHz, loop propagation delay of 15 ns and injection ratio less than −30 dB. Phase error variance values as low as 0.003 rad^2 in a bandwidth of 100 MHz, a mean time to cycle slip of 3×10^{10} s and SSB noise density of −94 dBc/Hz at 10 kHz offset were obtained for the same lasers in an heterodyne OIPLL configuration with loop propagation delay of 20 ns and injection ratio of −30 dB.**

***Index Terms*— Injection locking, linewidth, microwave optoelectronics, optical communication, optical phase-lock loop, semiconductor laser.**

I. Introduction

HOMODYNE and heterodyne laser synchronization techniques are required in a variety of optical communication [1], [2] and microwave photonic [3], [4] systems. A variety of synchronization techniques have been investigated, with the principles involved very similar to those used in electronic and/or microwave systems [5], [6]. Automatic frequency control (AFC) [7], [8] always involves finite frequency error and will not be considered further here. The most commonly used methods for exact frequency synchronization of a slave laser to an incoming master laser source are optical phase-lock loop (OPLL) [1], [3], [9] and optical injection locking (OIL) [10]–[12] systems.

In this paper, the limitations of these techniques are analyzed and a new locking technique, the optical injection phase-lock loop (OIPLL), which enables the limitations to be overcome, is described. The paper is organized as follows. In Section II, the OPLL rate equation is presented and the limitations imposed on phase noise suppression by the use of wide linewidth lasers investigated. Section III presents some of the important results obtained from the OIL laser rate equations and discusses the OIL range limitation at the high injection levels required to obtain low phase noise for wide linewidth lasers. In Section IV the OIPLL [13]–[15] is introduced and analyzed. The results show that the OIPLL can overcome the main operational problems in locking wide linewidth lasers, as the new system presents the phase noise suppression characteristics of the OIL configuration as well as the tracking characteristics of the OPLL architecture. Experimental results for equivalent homodyne OPLL, OIL, and OIPLL systems and an heterodyne OIPLL system are presented in Section V and the performance of the three locking techniques compared. Finally, general conclusions from the work are given in Section VI.

Manuscript received April 21, 1998; revised November 2, 1998. This work was supported by EPSRC, U.K., CNPq, and PRONEX/MCT, Brazil, and the U.S. ARO.

A. C. Bordonalli was with the Department of Electronic and Electrical Engineering, University College London, London, WC1E 7JE U.K. He is now with the Departamento de Microonda e Óptica, Faculdade de Engenharia Elétrica e de Computação, Universidade Estadual de Campinas, Caixa Postal 6101, Campinas, 13083-970, Brazil.

C. Walton and A. J. Seeds are with the Department of Electronic and Electrical Engineering, University College London, London, WC1E 7JE U.K.

Publisher Item Identifier S 0733-8724(99)01199-8.

II. The Optical Phase-Lock Loop

A. Time and Frequency Domain Analysis

Fig. 1 shows the general schematic diagram of an OPLL. In heterodyne systems, master and slave sources operate at different frequencies. The signals from the two sources are mixed on the active area of a photodetector, producing at its output a beat signal at a frequency corresponding to the frequency offset between the two sources. A phase detector compares the phase of the beat signal with that of an offset generator operating at a frequency close to that of the beat signal. A phase error signal is then produced at the output of the phase detector. The loop filter processes this signal and tunes the slave laser so as to minimize the phase error. The loop acquires lock when the frequency offset between the two optical sources is kept constant and equal to that of the offset generator.

By removing the components inside the dashed box and connecting the points A and B, the schematic diagram becomes the representation of an homodyne OPLL. In homodyne systems, master and slave sources oscillate at the same frequency and the photodetector is responsible for the phase detection. The slave laser phase control is similar to that of the heterodyne case and the loop acquires lock when the frequency offset between the lasers is zero.

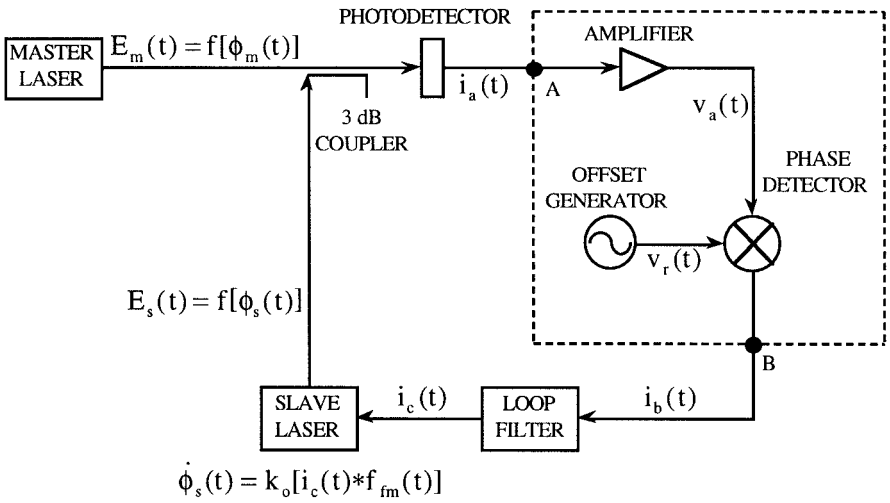

Fig. 1. Optical phase-lock loop. Dotted lines enclose additional components required for heterodyne operation.

From Fig. 1, assuming a balanced mixer as phase detector and matched impedances, the slave laser output can be written as:

$$\frac{d\phi_s(t)}{dt} = k_o k_d[\sin\theta(t) + n'(t)] * f_{fm}(t) * f(t) * f_{pdt}(t) * f_{phot}(t) * f_{\text{amp}}(f) * \delta(t - T_d) \quad (1)$$

where it is also assumed that the master laser electric field $E_m(t)$, the slave laser electric field $E_s(t)$ and the offset generator output voltage are given by, respectively

$$E_m(t) = E_{mo}e^{j[\omega_m t + \phi_m(t)]} \quad (2a)$$

$$E_s(t) = E_{so}e^{j[\omega_s^t + \phi_s(t)]} \quad (2b)$$

$$v_r(t) = A_r \cos[\omega_r t + \phi_r(t)] \quad (2c)$$

where E_{mo} (V/m), E_{so} (V/m), and A_r (V) are the amplitudes, ω_m, ω_s, and ω_r are the angular frequencies (rad/s) and $\phi_m(t)$, $\phi_s(t)$, and $\phi_r(t)$ are the phases (rad) of master and slave lasers and offset generator, respectively. The phase terms are written as

$$\phi_m(t) = \phi_{mo} + \gamma_m(t) \quad (3a)$$

$$\phi_s(t) = \phi_{so} + \gamma_s(t) \quad (3b)$$

$$\phi_r(t) = \phi_{ro} + \gamma_r(t) \quad (3c)$$

where ϕ_{mo}, ϕ_{so}, and ϕ_{ro} are the quiescent phases and $\gamma_m(t)$, $\gamma_s(t)$, and $\gamma_r(t)$ are the phase fluctuations of the master laser, slave laser and offset generator signal, respectively, k_o is the slave laser gain factor, $k_d = 1/2k_m A_r k_{co} k_{pd} k_{\text{amp}}$ is the phase detector output gain factor, k_m is the phase detector gain factor, k_{co} is a dimensionless term representing the efficiency in the wavefront overlap and k_{amp} is the amplifier gain. The photodetector gain factor is defined as $k_{pd} = 2R\sqrt{P_m R_s}$ (mA), where R is the photodetector responsivity (A/W), $P_m = E_{mo}^2 A_p/2z$ (W), $P_s = E_{so}^2 A_p/2z$ (W), A_p is the illuminated area of the photodetector (m^2) and z is the characteristic impedance of the medium (Ω).

In (1), $\theta(t) = \phi_{ms}(t) - \phi_r(t)$ is the phase error at the output of the phase detector, $\phi_{ms}(t) = \phi_m(t) - \phi_s(t)$ and $n'(t)$ is the quadrature representation of the photodetector shot noise [14]. The terms $f_{fm}(t)$, $f(t)$, $f_{pd}(t)$, $f_{\text{amp}}(t)$, and $f_{phot}(t)$ represent the impulse response of slave laser FM response, loop filter, phase detector, amplifier and photodetector, respectively, and $\delta(t - T_d)$ represents the loop propagation delay in the time domain.

By assuming that the phase error $\theta(t)$ is sufficiently small to allow the linearization of (1) and taking the Laplace transform of the result, the closed-loop transfer function for the OPLL system is

$$H(s) = \frac{\phi_s(s)}{\theta(s) + \phi_s(s)} = \frac{kF(s)F_{\text{out}}(s)F_{fm}(s)e^{-sT_d}}{s + kF(s)F_{\text{out}}(s)F_{fm}(s)e^{-sT_d}} \quad (4)$$

where the total loop gain $k = k_o k_d$ and the noise term has been neglected.

By considering an homodyne system and Fig. 1, (1)–(4) are valid observing that $k = k_o k_{pd} k_{co}$ as $k_d = k_{pd} k_{co}$, $f_{pd}(t) = 0$, $\phi_{ms}(t) = \theta(t)$, and $\omega_r t = \phi_r(t) = 0$.

B. OPLL Phase Noise Analysis and Stability

The major system noise sources can be identified from the analysis of Section II-A and their contribution calculated from the loop equations. First, it is assumed that the signals from master and slave lasers are locked and the system has been linearized. The phase difference between master and slave lasers and the phase error at the output of the phase detector are, respectively

$$\phi_{ms}(t) = \phi_{mo} - \phi_{so} + \gamma_m(t) - \gamma_s(t) \quad (5)$$

$$\theta(t) = \phi_{mo} - \phi_{so} - \phi_r(t) + \gamma_m(t) - \gamma_s(t). \quad (6)$$

In (5) and (6), ϕ_{so} is actually controlled by the loop to compensate the other phase terms by means of (1). Therefore, using (4), the Laplace transforms of the instantaneous values of $\phi_{ms}(t)$ and $\theta(t)$ are, respectively

$$\phi_{ms}(s) = [1 - H(s)][\Gamma_m(s) - \Gamma_s(s)] - H(s)[N'(s) - \phi_r(s)] \quad (7a)$$

$$\theta(s) = [1 - H(s)][\Gamma_m(s) - \Gamma_s(s) - \phi_r(s)] - H(s)N'(s) \quad (7b)$$

for an heterodyne system, where $\gamma_m(s)$, $\gamma_s(s)$, and $N'(s)$ are the Laplace transforms of $\gamma_m(t)$, $\gamma_s(t)$, and $n'(t)$, respectively. Similarly, for an homodyne system

$$\theta(s) = [1 - H(s)][\Gamma_m(s) - \Gamma_s(s)] - H(s)N'(s). \quad (8)$$

Equations (7) and (8) are a more complete set of equations for the OPLL as they include the system noise terms. By treating the laser phase noise as an ergodic process, the OPLL phase error spectrum can be obtained from either (7b) or (8) as

$$S_{\mathrm{OPLL}}(f) = [S_{PN\text{-}ML}(f) + S_{PN\text{-}SL}(f)]|1 - H(j2\pi f)|^2 + S_{SN}(f)|H(j2\pi f)|^2 \quad (9)$$

where $S_{PN\text{-}ML}(f)$ and $S_{PN\text{-}SL}(f)$ are the phase noise spectral density for master and slave lasers given by [16]–[18]

$$S_{PN\text{-}ML}(f) = \frac{\Delta F_{ml}}{2\pi f^2}, \quad S_{PN\text{-}SL}(f) = \frac{\Delta F_{sl}}{2\pi f^2} \quad (10)$$

where Δf_{ml} and Δf_{sl} are the master and slave FWHM laser linewidths, respectively, and $S_{SN}(f)$ is the phase translated shot noise spectral density given by [18]

$$S_{SN}(f) = \frac{e(P_m + P_s)}{2RP_mP_s}. \quad (11)$$

For an heterodyne configuration the phase translated shot noise is twice the result of (11) [18].

In order to illustrate the design features of the phase error spectrum, Fig. 2(a) and (b) shows the OPLL phase error spectrum calculated from (9) for ideal modified first- and second-order type II loop filters (with $F(s) = 1/(1 + s\tau)$ where τ is the filter time constant and $F(s) = (1 + s\tau_2)/s\tau_1$, where τ_1 and τ_2 are the filter time constants, respectively). The sum of the laser linewidths was 5 MHz and the loop delay 3 ns. The photodetector responsivity R was assumed to be 0.5 A/W. The loop gain was chosen as a parameter. The critical gain, defined as the gain value that causes loop oscillation, was obtained by setting $G(s) = \phi_s(s)/\theta(s) = -1$. The frequency response of the loop components other than the loop filter was assumed uniform. The time constants for both loops were chosen to give a zero-delay damping ratio of 0.707.

In Fig. 2(a) and (b), an increase in the loop gain results in an improvement of the low frequency phase noise suppression. This improvement should be extended to all frequencies if the loop parameters are such that the loop is operating inside a stable region. However, as the gain is increased toward its critical value, the OPLL becomes more susceptible to phase perturbations, as the phase margin of the loop is reduced. This effect can be seen from the peaking appearing in the phase error spectrum curve for high frequencies. As the loop gain tends to the critical value, the peak tends to infinity and the loop becomes unstable. Comparing Fig. 2(a) and (b), it is possible to notice that the second-order loop provides greater reduction in the low frequency phase noise than the modified first-order loop. This extra reduction is due to the inclusion of an integrator with high dc gain in the loop. Therefore, the static phase error of the second-order type II loop tends to zero, offering improved low frequency phase noise suppression. Integration of the phase error spectrum for all frequencies gives the OPLL phase error variance (σ^2).

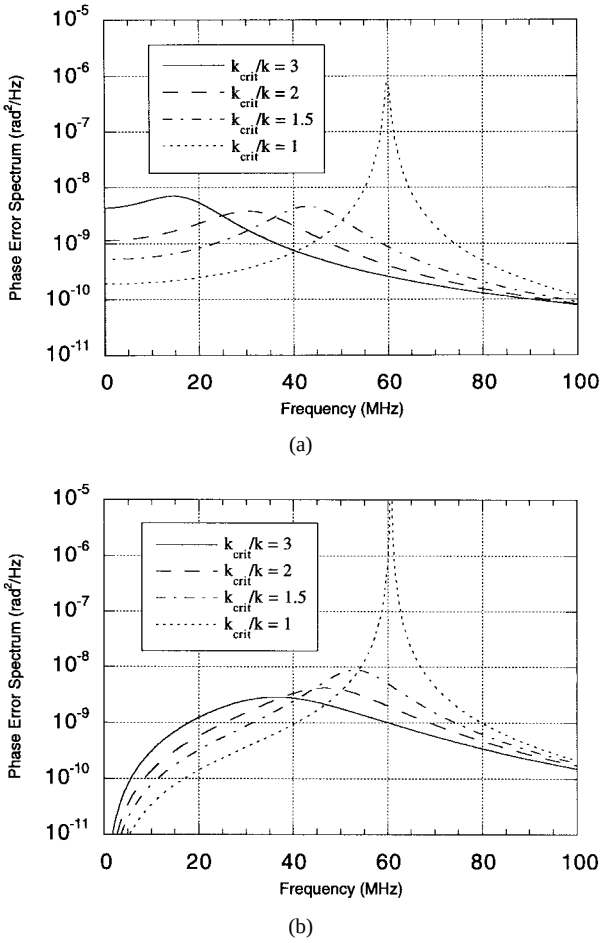

Fig. 2. Phase error spectra for (a) modified first- and (b) second-order type II optical phase-lock loops with zero-delay damping ratio of 0.707. Parameter: critical gain/loop gain. (Summed laser linewidths: 5 MHz; loop propagation delay: 3 ns; detector responsivity: 0.5 A/W.)

In Section II-A, the assumption made to solve the OPLL equation was that the phase error $\theta(t)$ is small enough to allow the linearization of the sinusoidal characteristic of the phase detector (photodetector). However, if the real response is taken into account, the phase detector gain can decrease dramatically depending on the mean phase error and, as a result, the loop can lose lock through cycle slipping [19], [23]. The average time between cycle slips for first-order and modified first-order loops and second-order type II loops are given by, respectively, [19]

$$T_{cs-I} \cong \pi \frac{e^{(2/\sigma^2)}}{4B_n}, \qquad T_{cs-II} \cong \frac{e^{(\pi/2\sigma^2)}}{B_n} \quad (12)$$

where B_n is the integration of $|H(j2\pi f)|^2$ for all frequencies. The probability of cycle slips is extremely dependent on the amount of phase error variance of the system [exponential term in (12)] and, therefore, on the laser phase noise.

The major phase noise source in the OPLL system is the laser phase noise. For acceptable phase noise suppression, the loop gain of the system should be as high as possible. However, as seen in Fig. 2, the loop gain is limited by the loop delay and, therefore, so is the phase noise reduction. Thus, the proper operation of an OPLL depend on the loop gain versus

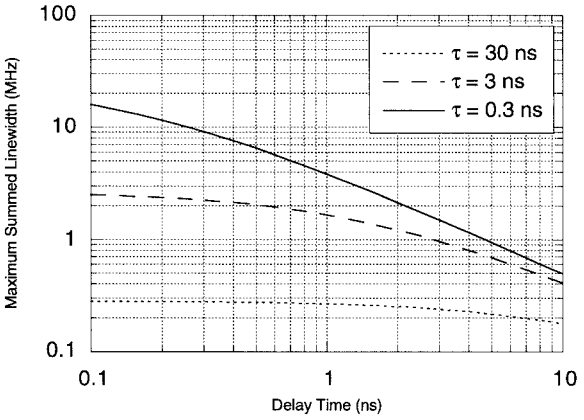

(a)

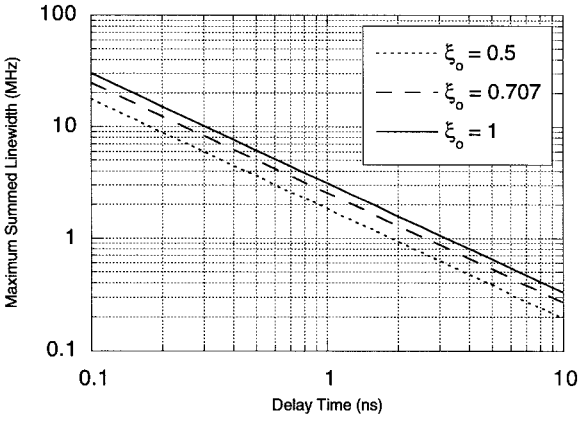

(b)

Fig. 3. Maximum summed linewidth versus delay time for mean time to cycle-slip of ten years for (a) modified first-order and (b) second-order type II OPLL systems. (Gain margin: 10 dB; detector responsivity: 0.5 A/W.)

delay relationship and on the correct choice of laser sources to be used in the system. The measurable parameter of a laser that is related to its phase noise is the laser FWHM linewidth. The laser linewidth can be related to the loop propagation delay by integrating (9) and substituting the result in (12) when T_{cs} is set to a fixed value. Fig. 3 shows the laser summed linewidth versus the delay time for (a) a modified first-order and (b) a second-order type II loop filters, where the loop gain for each value of delay is set 10 dB below its critical value. In order to ensure reliable operation for the system, the minimum T_{cs} was chosen to be ten years (315 Ms) [13], [23]. The other parameters are the same as those used in Fig. 2.

The modified first-order loop is slightly less restrictive than the second-order type II loop for values of loop delay beyond 0.5 ns [3], [23]. It is important to mention that a slight variation of the laser linewidth can change T_{cs} substantially. Clearly, from Fig. 3, the realization of OPLL's with wide linewidth lasers requires short propagation delays and wideband loop filters that may not be physically realizable.

III. Optical Injection Locking

A. Time and Frequency Domain Analysis

The injection locking of semiconductor lasers (Fig. 4) is a nonlinear phenomenon resulting from the injection of a master laser signal into a slave laser. The isolator in Fig. 4 prevents

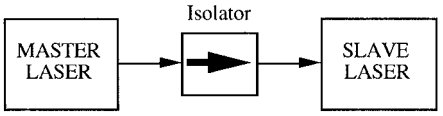

Fig. 4. Block diagram of an optical injection locking system.

both back reflections and slave laser emission from being coupled into the master laser. As a result of the injection, the slave laser frequency is pulled to that of the master laser and the system is kept locked while the free-running frequency difference between master and slave lasers is inside certain limits.

The interaction of the master laser electric field with the slave lasing medium can be analyzed from a coupled set of differential equations, describing the electric field and the carrier number. Assuming that the lasers are single mode and the system is locked, these equations for the slave laser can be expressed as [12], [20]

$$\frac{dI_s(t)}{dt} = \left\{\mathrm{Re}[G(t)] - \frac{1}{\tau_p}\right\} I_s(t) + \frac{2\sqrt{\eta I_s(t) I_m(t)}}{\tau_i} \cdot \cos\theta(t) + R + F_I \tag{13a}$$

$$\frac{d\phi_s(t)}{dt} = \omega_s - \omega_m + \frac{1}{2}\mathrm{Im}[G(t)] + \frac{1}{\tau_i}\sqrt{\frac{\eta I_m(t)}{I_s(t)}} \cdot \sin\theta(t) + F_\phi \tag{13b}$$

$$\frac{dN(t)}{dt} = \frac{I}{e} - \frac{N(t)}{\tau_s} - \mathrm{Re}[G(t)] I_s(t) + F_n \tag{13c}$$

where $G(t)$ is the complex gain per unit of time (s^{-1}), τ_p is the photon life time (s), η is a term representing the coupling efficiency of the master laser injected signal, τ_i is the round trip time of the electric field inside the laser structure (s), R_{spon} is the spontaneous emission rate (s^{-1}), I is the pumping current (A), τ_s is defined the carrier lifetime and e is the electronic charge (C). In (13), $I_s(t)$ and $I_m(t)$ are the slave and master laser photon numbers, respectively, $N(t)$ is the carrier number and F_I, F_ϕ, and F_n are the Langevin noise terms accounting for fluctuations of the number of photons, phase and carrier number [20], respectively.

The OIL rate equations are linearized and solved using the approximation of small perturbations around the steady state values of the system. The solutions then determine the stability of the steady-state operating conditions. After linearization and Laplace transformation, the transient solutions of the OIL rate equations can be written in matrix form as

$$\begin{bmatrix} s+A & -B & -C \\ D & s+H & -K \\ M & O & s+Q \end{bmatrix} \begin{bmatrix} \hat{i}(s) \\ \gamma_s(s) \\ \hat{n}(s) \end{bmatrix} = \begin{bmatrix} F_I'(s) \\ F_\phi'(s) \\ F_n'(s) \end{bmatrix} \tag{14}$$

where $A = R_{spon}/I_{so} - G_I I_{so} + \rho\cos\theta_o$, $B = 2\rho I_{so}\sin\theta_o$, $C = G_N I_{so}$, $D = \rho/2I_{so}\sin\theta_o$, $H = \rho\cos\theta_o$, $K = \alpha G_N/2$, $M = G_o + G_N\Delta N_o + G_I I_{so}$, and $Q = 1/\tau_s + G_N I_{so}$, I_{so}, I_{mo}, ϕ_{so}, ϕ_{mo}, and N_o are the steady state values and $\hat{i}_s(t)$, $\hat{i}_m(t)$, $\gamma_s(t)$, $\gamma_m(t)$, and $\hat{n}(t)$ are the deviations from the steady state values of $I_s(t)$, $I_m(t)$, $\phi_s(t)$, $\phi_m(t)$, and $N(t)$, respectively, $\Delta N_o = N_o - \tilde{N}_o$, $\tilde{N}_o$ represents the free-running steady state carrier number, $\theta_o = \phi_{mo} - \phi_{so}$ and

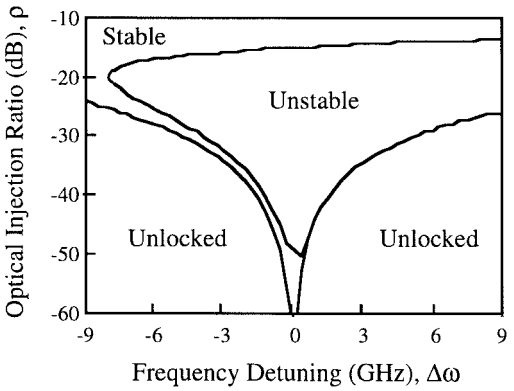

Fig. 5. Locking characteristics for a DFB laser (1550 nm, InP/InGaAsP, second-order grating, length: 322 μm; effective refractive index: 3.23; κ factor: 23/cm; facet reflectivities: 0.2% and 30%; linewidth enhancement factor: 5.4; internal loss: 50/cm).

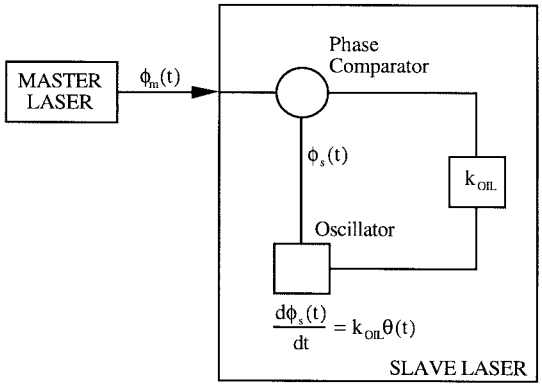

Fig. 6. Optical phase-lock loop representation of optical injection locking.

$\hat{\theta}(t) = \gamma_m(t) - \gamma_s(t)$. Second-order and cross-product terms of the deviations have been discarded. It is assumed that $G(t)$ can be written as $G(t) = G_o + G_N(1+j\alpha)[\Delta N_o + \hat{n}(t)] + G_I\hat{i}_s(t)$ within a first-order approximation and for operation above the laser threshold [12] where G_o is the free-running gain per unit of time (s^{-1}), $G_N = \partial G/\partial N$ is the differential gain related to the carrier number (s^{-1}), $G_I = \partial G/\partial I$ is the differential gain related to the photon number (s^{-1}) and α is the linewidth enhancement factor, which accounts for the electric field phase-amplitude coupling.

The condition for dynamic stability can be found from (14); the system will be dynamically stable if all the zeros of the coefficient matrix determinant are located in the left half of the complex s-plane [11], [12], that is, any perturbation of the steady state operating conditions of the injection locking process would die away and the system return to the equilibrium state. In general, the stability properties must be examined numerically. Fig. 5 shows an example of the expected locking characteristics for a DFB laser [21], calculated from the rate equations and using the stability criteria described above. The boundaries of the locked region are given by the locking range, defined from the steady state solutions of the OIL rate equations as

$$\Delta\omega = \omega_m - \omega_s = \frac{v_g}{2L}\sqrt{\frac{\eta P_{mo}}{P_{so}}}\,(\sin\theta_o - \alpha\cos\theta_o) \qquad (15)$$

where the proportionality between slave and master laser optical powers, P_{so} and P_{mo}, and their respective photon numbers is used and $\eta P_{mo}/P_{so}$ is defined as the injection locking ratio, L is the effective length of the slave laser cavity and $v_g = c/n_g$ is the group velocity, c is the speed of light and n_g is the group index. The OIL injection rate is defined as $\rho = v_g/2L\sqrt{\eta P_{mo}/P_{so}}$.

The injection locking is stable through the whole locking range for low values of injection locking ratio, below -50 dB. The stable region becomes extremely narrow as the injection locking ratio is increased and stable again over the whole range for very high injection ratio, beyond -10 dB. The instability is principally a result of the decrease in damping and increase in resonant frequency of the relaxation oscillations.

B. Phase-Lock Loop Model for Injection Locking and Noise Analysis

As already seen in Section III-A, the handling of the rate equations is not simple and the analysis of the dynamic behavior of the system becomes complicated. It is possible, however, to derive a simple model for the dynamic state of the stable injection locking process, based on its rate equations, which approaches the formalism of the phase-lock loop theory.

By assuming that the photon number of the laser field is instantaneously in equilibrium with the carrier population [22], that is, all the variation in the carrier population changes the refractive index and, therefore, the phase of the laser, by neglecting the Langevin terms and by assuming the small perturbation approximation, (13a)–(13c) can be combined, resulting in

$$\frac{d\gamma_s(t)}{dt} = k_{\mathrm{OIL}}[\gamma_m(t) - \gamma_s(t)] \qquad (16)$$

where the injection locking gain term k_{OIL} is defined as

$$k_{\mathrm{OIL}} = \frac{d\Delta\omega}{d\theta_o} = \rho(\cos\theta_o + \alpha\sin\theta_o). \qquad (17)$$

In the special case when the static phase error $\theta_o = 0$, $k_{\mathrm{OIL}} = \rho$. Fig. 6 shows the block diagram of a system that would be described by (16). The phase comparator represents the slave laser internal comparison of the slave laser phase with that of the master laser, delivering the phase difference between the two lasers at its output. The phase difference, or phase error, is amplified by the injection locking gain k_{OIL} and tunes the output phase of the oscillator, which represents the actual phase variation of the slave laser due to the injection locking process. Fig. 6 is very similar to the block diagram of an homodyne phase-lock loop. The phase comparator role is equivalent to that of the photodetector. The gain stage can be considered as the loop filter. Finally, the oscillator is equivalent to the locked slave laser. In fact, (16) can be obtained from (1) by setting $k_o k_d' = 1, n'(t) = 0$, as there is no real photodetector in the system, the loop impulse responses to k_{OIL}, the remaining impulse responses to "1" and removing the delay time term, as the injection locking process is seen to be unaffected by it. Thus setting the loop filter impulse response to k_{OIL}, which is equal to the loop filter transfer function, characterizes the system as first order.

The Laplace transform can be applied to the linearized (18) and $H_{\rm OIL}(s)$ is defined as the injection locking transfer function given by

$$H_{\rm OIL}(s) = \frac{k_{\rm OIL}}{s + k_{\rm OIL}}. \tag{18}$$

Using this phase-lock loop model for injection locking, it is possible to obtain the locking range of the injection locking system. The locking range or hold in range for a first-order loop is given by its dc gain. For the injection locking system, the dc gain is equal to $k_{\rm OIL}$, whose maximum value is obtained from (17). Therefore, the hold in range of the injection locking system is $\Delta\omega_{h\,\rm OIL} = \rho\sqrt{1+\alpha^2}$. This result agrees with the locking range expression obtained directly from the steady-state solutions of the rate equations where $|\Delta\omega| \leq \rho\sqrt{1+\alpha^2}$. It is important to point out that the result has to be corrected to consider the asymmetrical characteristics of the injection locking.

A great deal of simplification in the OIL noise analysis can be obtained by using the phase-lock loop approximation of the injection locking process presented above. In this approximation, the OIL rate equations are avoided and the Langevin terms are not expressly considered. However, their effect on the system can be taken into account if the phase terms of (16) are considered as the representation of the phase noise perturbations of the lasers, each one of them treated individually. Therefore, following Section II-B, the phase error spectrum for an OIL system can be written as

$$S_{\rm OIL}(f)[S_{PN\text{-}ML}(f)+S_{PN\text{-}SL}(f)]|1-H_{\rm OIL}(j2\pi f)|^2. \tag{19}$$

Fig. 7(a) and (b) shows the phase error spectrum for an OIL system for two different values of injection ratio, -50 and -30 dB, respectively, having the static phase detuning between the lasers as a parameter, calculated from (15). For this example, $\alpha = 5$, $n_g = 4.3$, and $L = 300$ μm. The phase noise suppression for the OIL system can be analyzed in two different ways. As expected, higher phase noise suppression can be achieved for higher injection ratio. By considering the same value of injection ratio, the system presents better noise characteristics as the phase detuning between master and slave lasers is varied from negative to positive values. The approximations made to obtain (19) do not predict the unstable locking region shown in Fig. 5 for high values of injection ratio. However, (19) can be used with good accuracy for phase or frequency detunings between master and slave laser that lie within the stable region of the locking range.

The phase error variance can be obtained from the phase error spectrum by integrating it over all frequencies. Fig. 8 shows the dependence of the phase error variance of the OIL system on frequency detuning for the same parameters and values of injection ratio used to calculate the plots of Fig. 7. The phase error variance sharply increases close to the borders of the locking range and its minimum value is achieved for frequency detunings close to zero. As expected from the results obtained from Fig. 7, the phase error variance is much smaller throughout the locking range for systems with higher injection ratios. For the example given, the difference between the minimum values of the curves for injection ratios

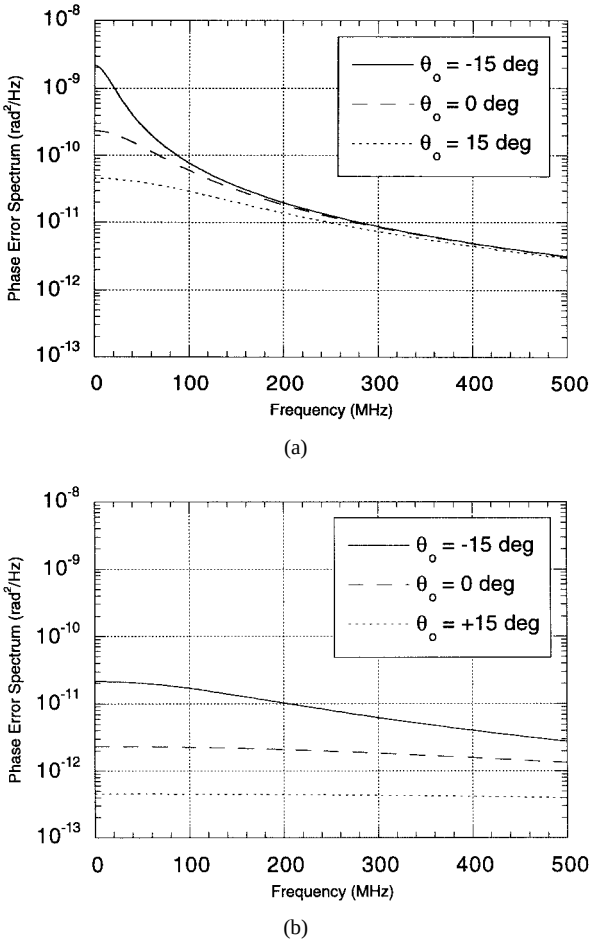

Fig. 7. Phase error spectrum for optical injection locking system with injection ratios of (a) -50 dB and (b) -30 dB. Parameter: phase detuning between master and slave lasers. (Summed laser linewidths: 5 MHz; linewidth enhancement factor: 5; group index: 4.3; effective cavity length: 300 μm.)

of -50 and -30 dB is around a factor of ten. The phase error variance calculated from (19) is invalid inside the unstable locking region, where the zero frequency detuning point would be located for high injection levels. This becomes evident during the experimental OIL observation, but Fig. 8 is still a useful tool to predict the phase noise suppression inside the stable region of an OIL system.

IV. Optical Injection Phase-Lock Loop

A. Time and Frequency Domain Analysis

The block diagram of the heterodyne OIPLL is shown in Fig. 9. Part of the light from the master laser is coupled into the modulator waveguide before being injected into the slave laser cavity. The slave laser is locked to a side-frequency of the modulated signal for the OIL part of the system. A similar side-frequency locking can be achieved by direct master laser modulation. The other part of the master laser light is combined with the slave laser output light on the active area of the photodetector for the OPLL part of the system, generating a beat signal at a frequency corresponding to the frequency offset between the two lasers. The phase of the beat signal is compared with that of the signal generator by a phase

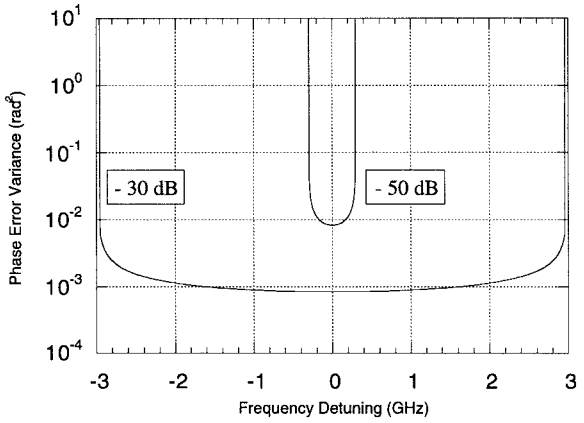

Fig. 8. Phase error variance for optical injection locking system. Parameter: injection ratio. (Summed laser linewidths: 5 MHz; linewidth enhancement factor: 5; group index: 4.3; effective cavity length: 300 μm.)

detector, which produces a phase error signal that is processed by the loop filter and tunes the slave laser to minimize the system phase error. Locking is acquired when the frequency offset between the two lasers is equal to the signal generator frequency. The block diagram of the homodyne OIPLL is obtained by removing the components inside the dashed box in Fig. 9. The slave laser phase is controlled in a similar way, with the phase error signal generated after the photodetector. Locking is acquired when the two lasers oscillate at same frequency.

Using the linearized injection locking model of Section III and the OPLL rate equation, the locked heterodyne OIPLL rate equation for the slave laser output phase is

$$\frac{d\phi_s(t)}{dt} = k_{\mathrm{OIL}} \sin \theta_{\mathrm{OIL}}(t) + k[\sin \theta_{\mathrm{OPLL}}(t) + n'(t)] * f_{fm}(t) * f(t) * f_{pd}(t) * f_{phot}(t) * f_{\mathrm{amp}}(t)\delta(t - T_d) \tag{20}$$

where the first term on the right-hand side represents the additional contribution of the OIL process to the OPLL system, $\theta_{\mathrm{OPLL}}(t) = \theta(t)$ and $\theta_{\mathrm{OIL}}(t) = \theta(t) + \theta_{\mathrm{diff}}$, where θ_{diff} is a phase term introduced phenomenologically to $\theta_{\mathrm{OIL}}(t)$ due to the fact that the instantaneous phase differences are measured at physically separate points. A more comprehensive discussion of θ_{diff} will be included later.

For simplicity, it is first assumed that θ_{diff} is set to zero and that the phase difference is small enough to allow the linearization of the sinusoidal terms in (20). Under the assumption that $k_{\mathrm{OIL}} = \rho$, and taking the Laplace transform of the linearized (20), the closed-loop transfer function for the OIPLL system is given by

$$H_c(s) = \frac{\phi_s(s)}{\theta(s) + \phi_s(s)} = \frac{\rho + kF(s)F_{\mathrm{out}}(s)F_{fm}(s)e^{-sT_d}}{s + \rho + kF(s)F_{\mathrm{out}}(s)F_{fm}(s)e^{-sT_d}}. \tag{21}$$

B. OIPLL Phase Noise Analysis and Stability

As the OIPLL consists of the combination of OPLL and OIL systems, the noise source analysis carried out in the previous Sections can be extended to this system and the major noise sources of the system can be identified. Equation (3) defined the master and slave laser phase terms, where the first representations of the laser phase noise were introduced. In (1), $n'(t)$ was considered as a noise source associated with photodetector shot noise. The contribution of the major noise sources to the system can be calculated from the OIPLL equations. First, it is assumed that the signals from master and slave lasers are locked and the system has been linearized. The differential phase is assumed zero. Following the same procedure as in Section II-B, the phase error spectrum for an OIPLL system is given by:

$$S_{\mathrm{OIPLL}}(f) = [S_{PN\text{-}ML}(f) + S_{PN\text{-}SL}(f)]|1 - H_c(j2\pi f)|^2 + S_{SN}(f)|H_c(j2\pi f)|^2. \tag{22}$$

For an homodyne system, the same simplifications as the ones for the OPLL system can be applied to (22). The phase error variance can be obtained from the phase error spectrum by integrating it over all frequencies.

The analysis of the performance of the OIPLL system can be better seen by means of comparison of the phase error spectrum of the new system and the results obtained for the equivalent OIL and OPLL configurations used individually. Fig. 10 shows the phase error spectrum for a second-order type II OIPLL and the equivalent OIL, OPLL and free-running laser systems [13], [14]. The second-order type II OIPLL system would ensure zero static phase error and, therefore, reinforce the assumptions made for the OIPLL rate equation. The OPLL gain was set at the critical stability value for 3 ns loop delay. It can be seen that addition of the OIL path improves the loop stability and hence removes the phase noise peaking from the spectrum, allowing systems with high loop gains for much longer loop delays than the equivalent OPLL. The system becomes stable as the injection locking adds a delay-unaffected extra damping factor to the OPLL part of the system.

From Fig. 10, the main phase noise contribution for the OIPLL appears to be beyond 10 MHz, where its phase error spectrum tends to follow the response of the equivalent OIL process. Therefore, the injection locking part of the OIPLL is mainly responsible for the control of the phase noise, which relaxes the phase-lock loop bandwidth requirements, allowing the use of conventional electronic components. The use of a second-order type II loop filter can be seen as creating a phase reference for the injection locking around zero static phase error, compensating the long term phase fluctuations (below 10 MHz), which ensures that the injection locking process remains within its stable operation region. Although the OIL contribution to the OIPLL system does not give the best phase noise suppression that is possible with an OIL system used alone, the OIPLL enables the OIL part of the system to operate stably, even at the moderate to high injection powers required for effective phase noise suppression with wide laser linewidths. This results in a system with low values of phase error variance over a much wider stable locking range, provided by the large dc gain of the phase-lock feedback circuit. Due to the improved phase noise suppression, the OIPLL possesses a much longer mean time between cycle slips than the equivalent OPLL system.

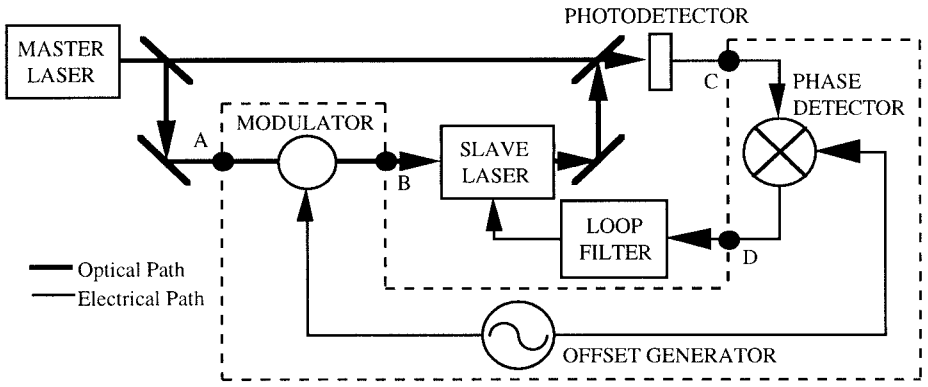

Fig. 9. Optical injection phase-lock loop block diagram. Dotted lines enclose additional components required for heterodyne operation.

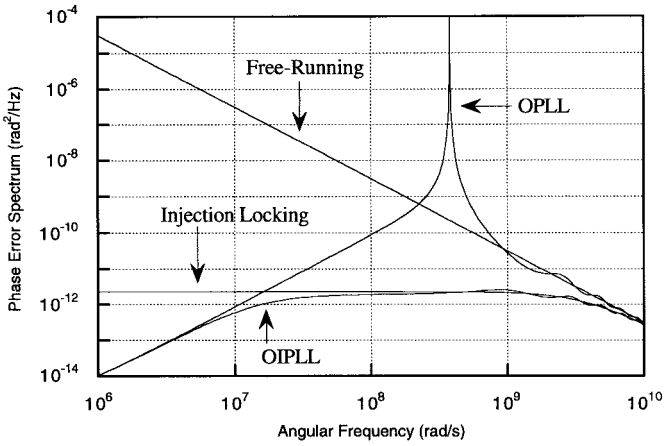

Fig. 10. Phase error spectra for various optical locking techniques, with injected power ratio of -30 dB and total loop propagation delay of 3 ns. (Summed laser linewidths: 5 MHz; linewidth enhancement factor: 5; group index: 4.3; effective cavity length: 300 μm; zero delay damping ratio: 0.707; loop natural frequency: 245.3 Mrad/s; OPLL gain: critical.)

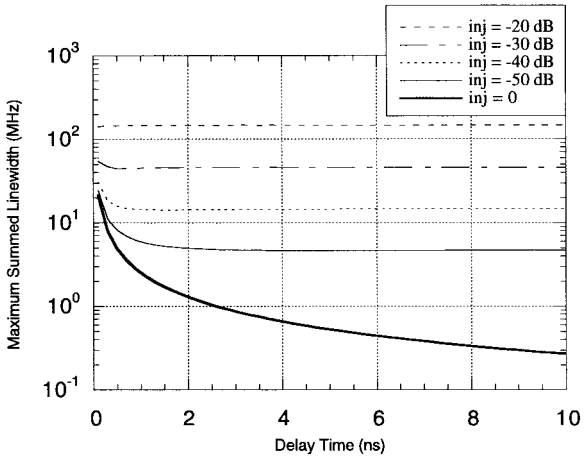

Fig. 11. Maximum OIPLL summed linewidth versus delay time. Parameter: injection ratio. The loop gain is set to be the maximum stable gain for the equivalent OPLL. (Summed laser linewidths: 5 MHz; linewidth enhancement factor: 5; group index: 4.3; effective cavity length: 300 μm; zero delay damping ratio: 0.707; loop natural frequency: 245.3 Mrad/s; integration bandwidth: 1 GHz; mean time to cycle slip: ten years.)

Using the same criteria as those used to calculate Fig. 3, it is possible to obtain a plot of the maximum summed linewidth versus delay for the OIPLL and compare the results with the equivalent OPLL, Fig. 11. The restrictions imposed on the linewidth of the lasers by the loop delay are considerably relaxed and the use of commercially available semiconductor lasers without line-narrowing techniques is seen to be possible.

The effect of finite differential phase, θ_{diff}, on the OIPLL performance is now analyzed. In practical systems, the difference in path lengths results in phase shifts at the two separate phase comparison points of Fig. 9, leading to different phase error measurements and, therefore, competition between the two locking processes and possible system instability. The differential phase can be defined for heterodyne and homodyne cases as, respectively

$$\theta_{\text{diff-het}} = \omega_m(t_b + t_c - t_a) + \omega_r(t_b + t_c + t_d + t_f - t_e) \tag{23a}$$

$$\theta_{\text{diff-hom}} = \omega_m(t_b + t_c - t_a) \tag{23b}$$

where t_a, t_b, t_c, t_d, t_e, and t_f are the time intervals corresponding to the signals travelling the paths from master laser to photodetector, from master laser to slave laser, from slave laser to photodetector, from photodetector to phase detector, from offset generator to master laser (assuming side-frequency locking to a directly modulated master laser) and from offset generator to phase detector, respectively.

In addition to the instabilities that can be caused by the existence of a path mismatch in the system, the maximum master laser frequency detuning will also be limited. Good OIPLL system performance is achieved only if the differential phase is small. The effect of the path mismatch and master laser detuning is shown in Fig. 12. For a path mismatch where θ_{diff} is $2\pi n$, master laser frequency detuning causes θ_{diff} to vary from the $2\pi n$ value toward quadrature and the OIPLL phase noise suppression starts deteriorating. If the detuning is such that the θ_{diff} variation is small, the system will retain good phase noise control. For instance, for a master laser frequency detuning of 42 GHz in an homodyne system, an optical path mismatch of the order of 0.1 mm would ensure only 5° of θ_{diff} variation and less than 0.4% of decrease in the injection locking contribution, represented by ρ in (21). An elegant solution to the path mismatch problem would be the monolithic integration of the system, where optical path matching to within the laser wavelength is possible, allowing frequency tuning of the master laser over teraHertz ranges.

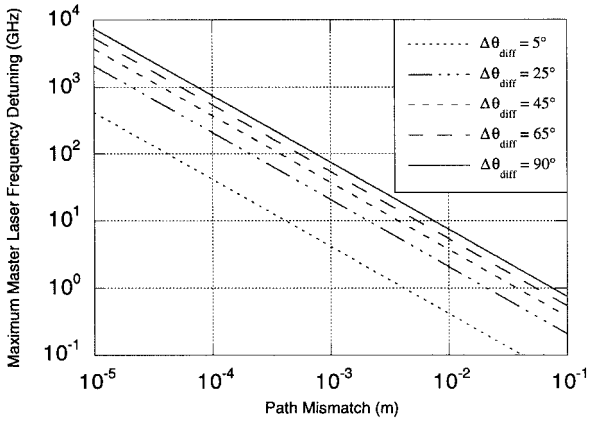

Fig. 12. Maximum master laser frequency detuning versus path mismatch for optical injection phase-lock loop.

V. Experimental Results

Experimental homodyne and heterodyne OIPLL's were constructed to test the predictions of Section IV. Fig. 13(a) shows the homodyne experimental OIPLL setup. Part of the light emitted by the master laser (ML) is injected into the slave laser (SL) cavity. The isolators I1 and I2 prevent the coupling of slave laser emission and back reflections to the master laser. The angle of the half-wave plate H1 controls the injection level by varying the output light ratio of the polarizing beam splitter PBS1. I3 (which has the front polarizer removed) and H2 ensure ML and SL beam polarization matching at 0°. The other part of the ML beam is reflected by PBS1 and by the mirror M, being fully transmitted through PBS1 toward the nonpolarizing beam splitter (NBS) after passing twice through the quarter-wave plate Q1. The polarization direction of the SL emission is 0°. After H2 and I3, the SL beam polarization is 90° and, therefore, it is fully reflected by PBS1 toward NBS. NBS divides the two beams without changing their polarization state. The transmitted output passes through the combination of H4 and PBS3, ensuring the same polarization for the beams being coupled into the fiber coupler FC and, therefore, high efficiency in the wave front overlap. An optical fiber cable with a 3-dB coupler is used to take the signal from FC to both a Fabry–Perot interferometer FPI (Burleigh HF-1500-2) and a lightwave signal analyzer LSA (HP 70810B). The NBS reflected output goes to the balanced receiver of the OPLL part of the system. The combination of Q2, H3, and PBS2 ensures power balance and high efficiency in wave front overlap on the active area of the photodetectors PH1 and PH2. The signals generated by the photodetectors are summed and amplified by a first stage amplifier and integrated by a second-order type II filter with transfer function $F(s) = (1 + s\tau_2)/s\tau_1$. The filter output is combined with the slave laser bias and tunes the slave laser to minimize the phase error in the loop. Fig. 13(b) shows the heterodyne experimental OIPLL set-up. In this case, the optical components of Fig. 13(a) after PBS1 are rearranged and the balanced receiver removed. A second fiber coupler (FC2) is added to the system to allow the ML and SL signals to illuminate a 20-GHz bandwidth photodetector (PH3). H3 and PBS2 ensure beam polarization matching at both FC inputs. A signal generator (SG) provides a modulation signal

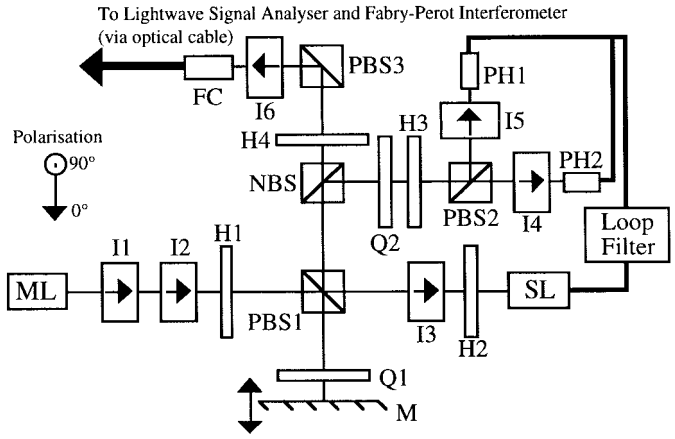

(a)

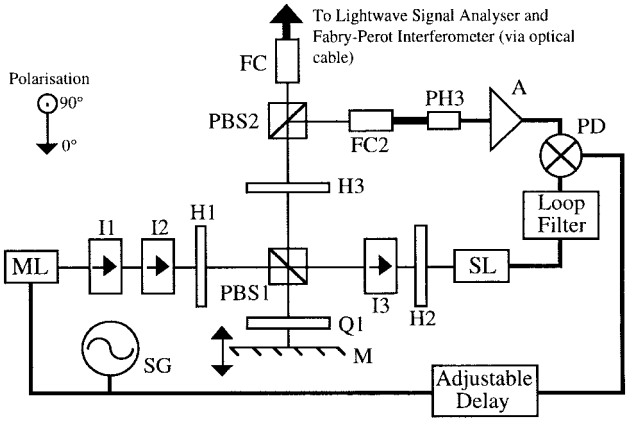

(b)

Fig. 13. Experimental optical injection phase-lock loops. (a) homodyne loop and (b) heterodyne loop. ML: master laser; SL: slave laser; L: lens; ISO: isolator; H: half-wave plate; Q: quarter-wave plate; PBS: polarizing beam splitter; M: mirror mounted on a translation stage; PH1 and PH2: photodetectors; PD: phase detector; SG: signal generator; A: amplifier; FC: fiber coupler.

for the ML and a reference signal for the OPLL part of the system. The adjustable delay stage enables the differential path length between phase comparison points and hence differential phase to be adjusted. The PH3 output signal is amplified by a microwave amplifier (A) and its phase compared with that of the reference signal by a phase detector (PD). The phase error signal at PD output is processed by a second-order type II filter tuning the slave laser to control the phase error.

A. The OPLL Experiment

In order to perform an homodyne OPLL experiment the angular position of H1 [see Fig. 13(a)] was set so that the master laser light was completely reflected by PBS1 thus eliminating injection into the slave laser cavity. The laser beams were then aligned to maximize wavefront overlap.

The master and slave lasers, two buried heterostructure 1.546 μm wavelength DFB devices, were biased at $2.75 \times I_{th}$ and $2.2 \times I_{th}$, respectively, where I_{th} is the threshold current for each laser. After balancing, the measured photocurrents at the output of each photodetector were 420 μA and 360 μA due to master laser and the slave lasers, respectively. The

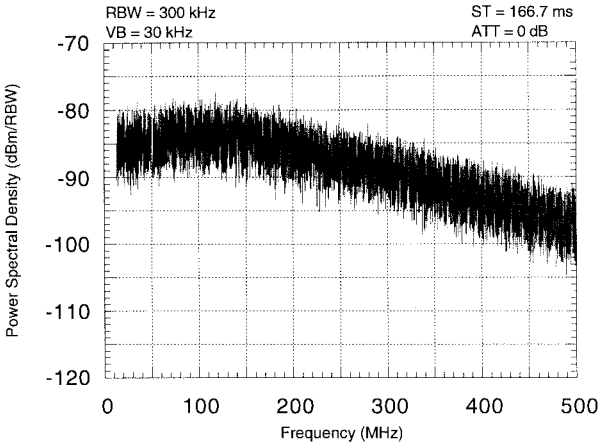

Fig. 14. Detected homodyne optical phase-lock loop power spectrum. The loop parameters are such that $\xi_o = 0.76$.

photodetector responsivities were 0.89 A/W. The measured effective photodetector gain factor and the effective coupling efficiency were 380 μA/rad and 0.5, respectively.

The Fabry–Perot interferometer (Burleigh FPI-HiFase HF-1500-2) permits the observation of the laser optical spectrum with sufficient resolution to make quantitative measurements of the longitudinal mode frequency variation, making it possible to characterize the locking range for the different locking systems. The lightwave signal analyzer (HP 70810B) allows the measurement of the OPLL, OIL, and OIPLL output signal spectrum. The electrical power measured by the lightwave signal analyzer for the master laser was -54.8 dBm and for the slave laser was -51.4 dBm. Under these conditions and assuming that the load for the photodetector of the lightwave analyzer is 50 Ω, the coupling efficiency $k_{co\text{-}lsa}$ and photodetector gain factor $k_{pd\text{-}lsa}$ for the lightwave signal analyzer measurement were 0.5 and 10 μA/rad, respectively.

The OPLL phase noise spectrum was obtained from the lightwave signal analyzer measurements and is shown in Fig. 14 for a total loop gain of 4.4 Grad/s. The loop filter chosen was a second-order type II filter. The total loop gain and time constants ($\tau_1 = 0.43$ μs and $\tau_2 = 15$ ns) gave a zero delay damping ratio $\zeta_o = 0.76$, close to the value of 0.707 assumed in the theory sections.

It can be seen that the OPLL system cannot provide any substantial suppression of the laser phase noise. This was expected from the fact that the values of laser summed linewidths, in this case 36 MHz, and the delay time of the system, estimated to be 15 ns from the nominal delays of the electronic components plus the actual size of the loop, exceed those required to meet the cycle slipping criterion, Fig. 3. The amount of cycle slipping after the loop was closed is responsible for the broadening of the OPLL power spectrum, leading to poor system phase noise control and strong tendency for the loop to lose lock.

The phase error variance for the OPLL system numerically calculated by numerical integration of the phase error spectrum, Fig. 14, was 0.974 rad^2. This value is well beyond the linear range of the OPLL analysis assumptions. Although this implies that the result given above is not accurate, the approximation is good enough to illustrate the behavior predicted in the OPLL analysis. As expected, this result confirms the poor phase noise suppression performance of such an OPLL configuration for wide linewidth lasers and long loop propagation delays.

B. The OIL Experiment

In order to characterize the OIL system and compare the results with the theoretical predictions of Section III, an OIL experiment was carried out. The parameters obtained were subsequently used to characterize the OIL path within the OIPLL system.

The set-up for the OIL experiment is the same as that of Fig. 13(a). The amount of injected power and, therefore, the injection ratio, is controlled by H1 rotation. The system injection ratio is estimated for different H1 angles from the measured slave laser photocurrent produced by the master light injection, the measured OIL locking bandwidth by the Fabry–Perot interferometer and (15). For this calculation the measured α was 3.9, the total slave laser power was 4.5 mW, the round-trip time τ_i was 7 ps and the responsivity of the slave laser R_{SL} was assumed to be 0.9 A/W.

The power spectral density was measured by the lightwave signal analyzer for each value of H1 angle and the data stored. In each case, the master laser was tuned to bring the two laser frequencies close enough to allow locking. When the lasers are locked, it was observed that as the frequency detuning between the lasers is varied, the power spectrum for the OIL process changes. This behavior is expected from the theoretical analysis, as the phase noise suppression is a function of the injection ratio and detuning.

The sequence of plots in Fig. 15 show the power spectra measured by the lightwave signal analyzer for different injection ratios and detunings. The detunings were obtained from measurements of the master and slave laser frequency difference with and without injection, using the Fabry–Perot interferometer, which were later compared with the theoretical predictions obtained from fitting the measured OIL power spectrum curves.

Fig. 15(a) shows the spectrum for a very low level of injection. As the injection is increased, the phase noise suppression becomes better. For a given value of injection ratio, the detuning determines the best OIL performance for the measured plots, as expected from the OIL phase noise analysis. Under the laser bias conditions used, $k_{co\text{-}lsa}$ and $k_{pd\text{-}lsa}$ were the same as those for the OPLL experiment. For a measurement bandwidth of 500 MHz, the measured phase error variances are 0.272, 0.04, 0.017, 0.016, and 0.004 rad^2 for Fig. 15(a), (b-1), (b-2), (c-1), and (c-2), respectively.

C. The Homodyne OIPLL Experiment

In Section V-A and B, the experimental results of the separate OPLL and OIL systems were presented. The next step is to combine the OPLL and OIL systems and analyze the experimental results for an homodyne OIPLL configuration [15]. The main problem in OIPLL implementation is the differential phase resulting from the difference in the optical paths

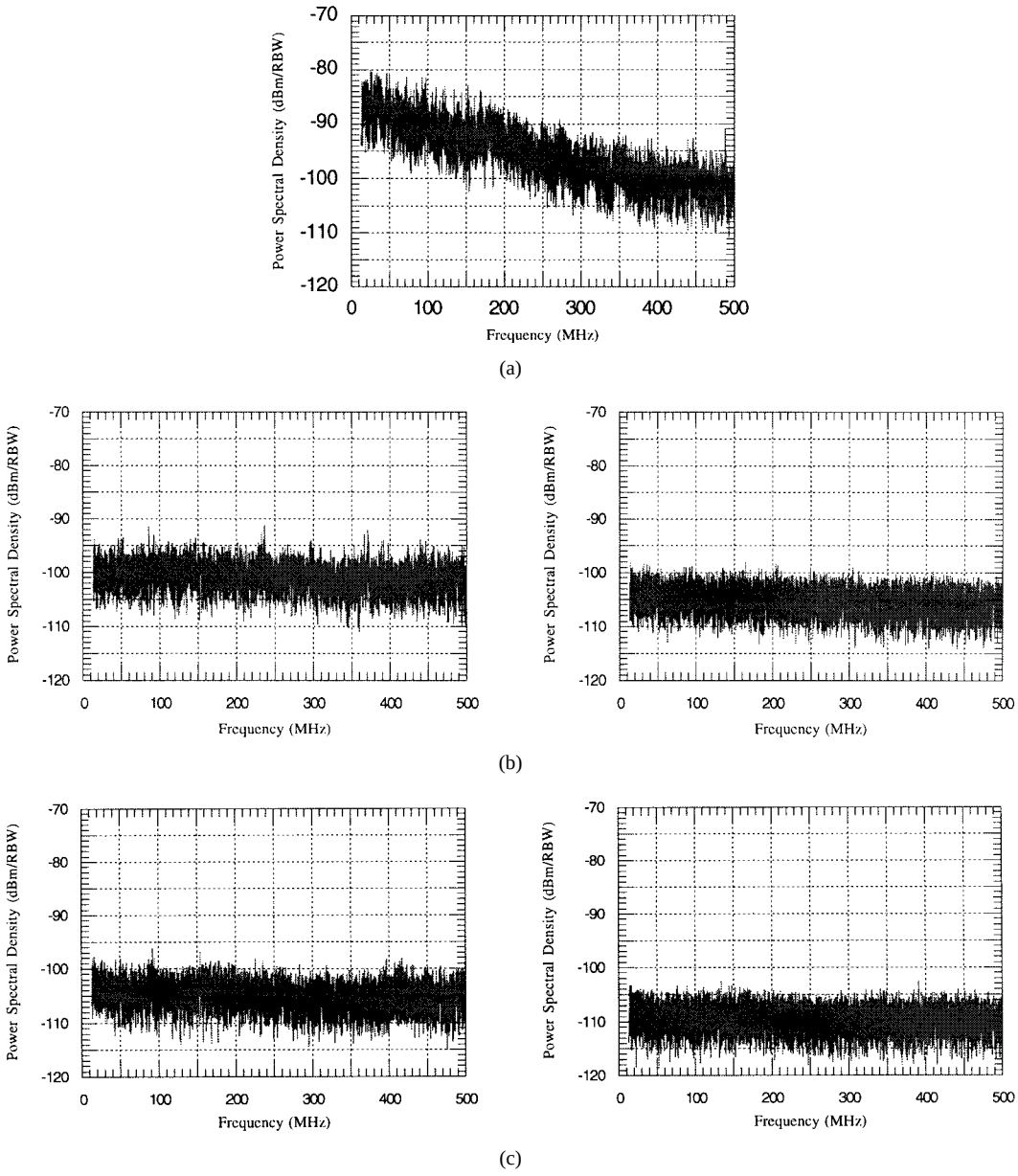

Fig. 15 Detected power spectrum of optical injection locking system for different values of injection ratio and detuning. The lightwave signal analyzer is set to lightwave-electrical mode: resolution bandwidth 300 kHz; video bandwidth 30 kHz; sweep time 166.7 s; attenuation 0 dB. (a) Injection ratio -47 dB, detuning -6.7°; (b) Injection ratio -36.4 dB, (b-1) detuning -3°, (b-2) detuning 7°; (c) Injection ratio -31.4 dB, (c-1) detuning -4°, (c-2) detuning 7°.

from master laser to photodetector and from master laser to slave laser and slave laser to photodetector. In order to achieve path matching the OIPLL was reconfigured as a Michelson interferometer. The longitudinal mode frequency was then tuned by temperature and observed using the Fabry–Perot interferometer while the oscillations in optical power were observed on an optical power meter. For long path mismatches, the ML intensity oscillated with tuning. After that, the path mismatch was corrected by means of adjusting the drive and piezoelectric elements located in the translation stage of the mirror mount (Fig. 13). The procedure was repeated until no intensity fluctuations could be detected. The master laser tuning interval was beyond 170 GHz of frequency scan. Path matching to less than 20 μm was achieved and the influence of the differential phase θ_{diff} was kept below 5° for more than 100 GHz of master laser frequency variation.

The OIPLL system configuration is the same as that for the OPLL experiment, but with H1 rotated to allow injection to occur. During the experiment, the parameters of the loop and the injection locking process (laser bias, injection ratio, loop gain, etc.) were kept the same to allow comparison of the results of the three locking techniques. This is possible as the three experiments can be performed in succession using the same experimental setup.

Fig. 16 shows the sequence of power spectral density plots measured by the lightwave signal analyzer for different injection ratios. Unfortunately, measurements at higher values of injection ratio than the ones presented were not possible due to the noise floor of the instrument. It can be seen that the low injection measurement presents a characteristic very similar to that presented by the OPLL system. That is expected as the injection influence is small and the system

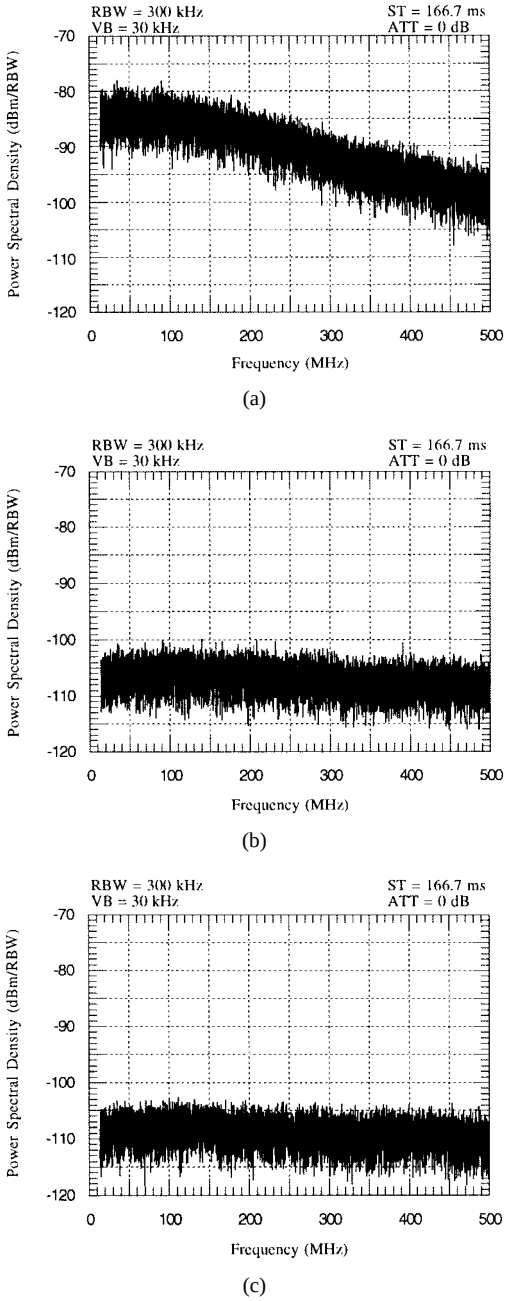

Fig. 16. Detected power spectrum for the homodyne OIPLL system for injection ratios (a) −47 dB, (b) −36.4 dB, and (c) −31.4 dB. RBW: resolution bandwidth; VB: video bandwidth; ST: sweep time; ATT: attenuation.

still presents the cycle slipping problem of the phase-lock technique. However, as the injection ratio is increased, the influence of the master laser injected power contributes to the laser frequency synchronization process, reducing the phase noise level.

Fig. 17 shows the comparison between the OPLL and the OIPLL results for the same loop parameters as those described in Section II-B and injection ratio −31.4 dB. This figure also shows the expected theoretical plot for the OIPLL system. It can be seen that the addition of the injection locking path improves the poor phase noise suppression of the OPLL system. Also, there is good agreement between the modeled and experimental OIPLL results, as, in this case, the linear assumptions made during the theoretical analysis are valid.

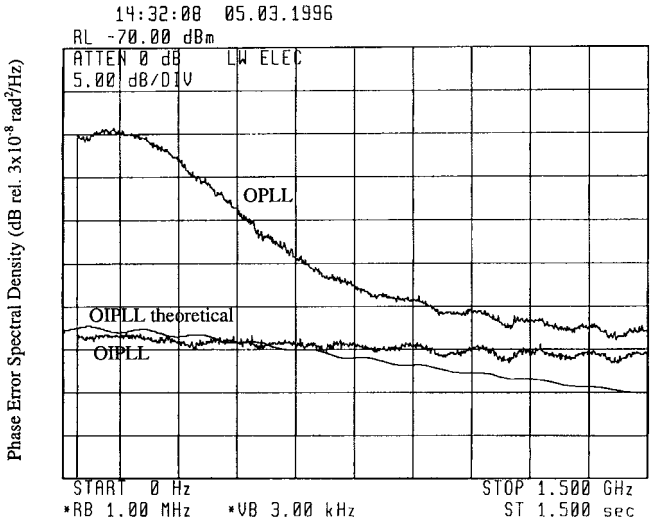

Fig. 17. Power spectral densities for homodyne OPLL and OIPLL systems. Injection ratio is −31.4 dB. Reference level corresponds to 3×10^{-8} rad^2/Hz.

The phase error variance was measured for different frequency detunings between master and slave lasers. This enabled the locking bandwidth and variation in phase noise suppression for the OIPLL system to be checked across the locking range. As theoretically predicted, it was observed that the OIL system presented an unstable region for certain values of detuning between master and slave laser frequencies above a critical level of injection. Fig. 18 shows the phase error variance measured in 500 MHz bandwidth as a function of the detuning between master and slave lasers for different injection ratios, obtained from the power spectral density measurements for OIL and OIPLL systems. In Fig. 18(a), the OIL measured detuning corresponds to the power spectral density plot of Fig. 15(a). In Fig. 18(b), the OIL measured detuning correspond to the power spectral density plots of Fig. 15(b). Fig. 18(c) presents the phase error variance values obtained from Fig. 15(c) and other measurements [15]. Although it is possible to achieve lower values of OIL phase error variance for given values of injection ratio and detuning than the ones achieved by the OIPLL system, the detuning that is possible before the OIL system becomes unstable severely restricts the OIL locking range to a very narrow region, for instance, less than 1.2 GHz for −31.4 dB injection ratio. For higher injection ratios, the OIPLL was able to maintain low values of phase error variance for a much wider stable locking range, exceeding 20 GHz for all injection levels, and limited only by saturation of the loop filter electronics. Fig. 18(a)–(c) compares the phase error variance predictions from the theoretical OIPLL and OIL models of Sections III and IV with the experimental results. It can be seen that it is possible to obtain good agreement between the theory and experimental cases for moderate and high injection ratios. This is expected as the injection locking part of the system suppresses most of the high frequency phase noise, making the linear approximations used valid.

D. The Heterodyne OIPLL Experiment

The homodyne experimental setup was modified to give the heterodyne experiment of Fig. 13(b) [24]. The same master

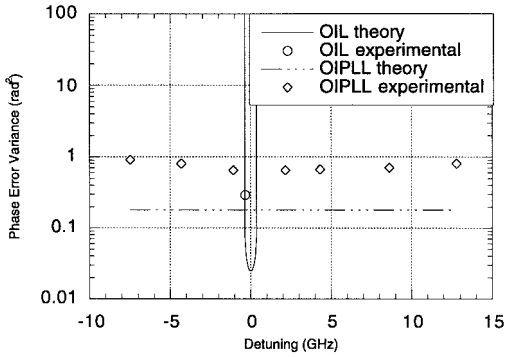

(a)

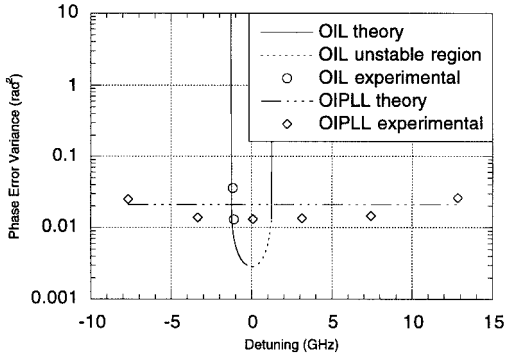

(b)

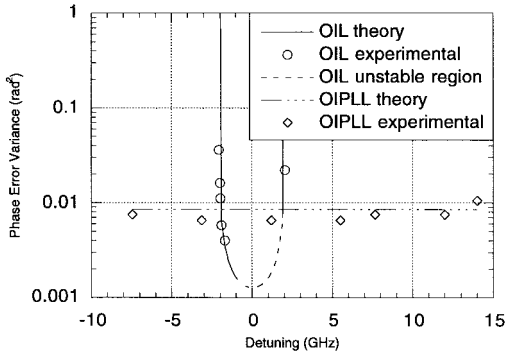

(c)

Fig. 18. Phase error variance for homodyne OIL and OIPLL systems as a function of the detuning between master and slave laser frequencies. Injection ratios (a) −47 dB, (b) −36.4 dB, and (c) −31.4 dB. Measurement bandwidth 500 MHz.

and slave lasers were biased at around $2.75 \times I_{th}$ and $2.1 \times I_{th}$. In order to minimize the effect of θ_{diff}, close path matching was obtained as in the homodyne OIPLL and by careful adjustment of the electrical path length from oscillator to mixer.

The first experimental step was to perform the sideband OIL experiment. H1 was rotated such that the level of upper sideband injection ratio was −30 dB. Note that the injection ratio of the master laser fundamental line is considerably higher at −23 dB due to its larger power. In these experiments, the offset frequency had to be greater than 6 GHz to prevent the slave laser locking to the master laser fundamental for these injection levels. Fig. 19 shows the detected microwave signal. The noise single sideband power spectral density was measured as −94 dBc/Hz at 10 kHz offset—virtually equal to

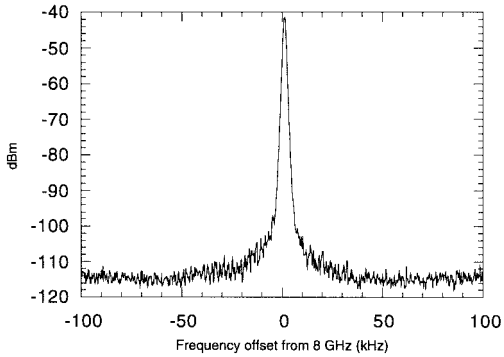

Fig. 19. Detected spectrum for the sideband injection locking system. Injection ratio: −30 dB. Span = 200 kHz, resolution bandwidth = 300 Hz.

the reference oscillator noise power spectral density of −95 dBc/Hz. However, the OIL locking range, measured by tuning the master laser by temperature, was less than 2 GHz [24].

Next, the phase-lock path, with measured loop delay of 20 ns, total loop gain 50 Mrad/s and active loop filter time constants $\tau_1 = \tau_2 = 100$ ns, was added to the system and measurements of the OIPLL performance were made. Fig. 20 shows the 8 GHz beat between master and slave lasers, with a power spectral density of −94 dBc/Hz at 10 kHz offset and variance of 0.003 rad^2 in a bandwidth of 100 MHz (limited by lightwave signal analyzer noise floor). The hold-in range was increased to greater than 24 GHz, and the variation in heterodyne frequency by reference oscillator tuning was greater than 200 MHz, limited by loop microwave component bandwidth.

Harmonic locking was also shown to be possible with the OIPLL system. Since modulation of the master laser results in both intensity modulation (IM) and frequency modulation (FM), multiple side frequencies are generated. Injection locking to the second harmonic (16 GHz) offset side frequency is therefore possible, and was achieved with a locking range of less than 1 GHz. With the addition of the OPLL, the hold-in range was increased to 4 GHz. The hold-in range is lower than for fundamental locking because the injection ratio for the 16 GHz sideband is smaller, at −37 dB, resulting in reduced OPLL loop gain.

Finally, it was observed, that in an uncontrolled laboratory environment, both homodyne and heterodyne OIPLL's remained locked for periods of several hours, with no degeneration in phase noise suppression performance. From the measurements of phase error variance, it is estimated that the mean time to cycle slip for the heterodyne OIPLL is 3×10^{10} s, or over 900 years.

VI. Conclusions

An optical locking system combining both injection locking and phase locking techniques, the OIPLL, has been analyzed and demonstrated experimentally for the first time. The system configuration permits the use of wide linewidth semiconductor lasers in a type II loop design with large loop propagation delay while maintaining good stability and low phase error variance.

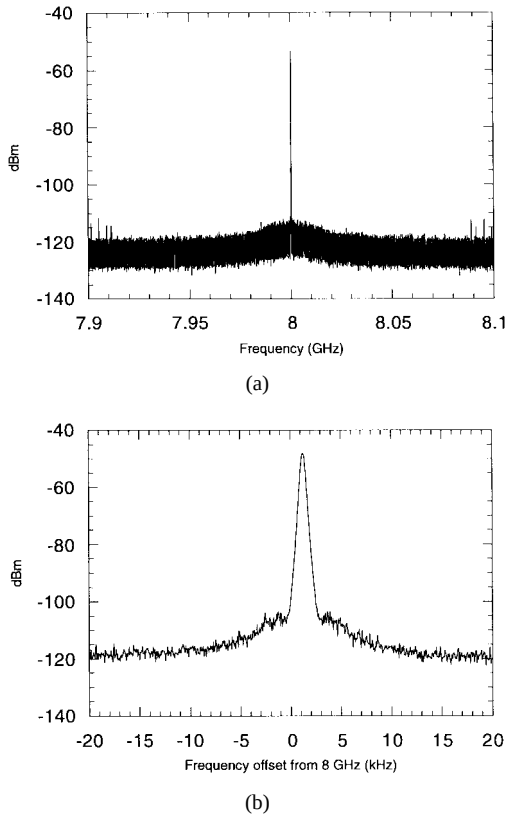

Fig. 20. Detected spectra for the heterodyne OIPLL system, injection ratio: −30 dB. (a) span = 200 MHz, resolution bandwidth = 3 kHz and (b) span = 20 kHz, resolution bandwidth = 300 Hz.

From the OPLL analysis, loop propagation delay was seen to be the restricting factor on the loop bandwidth and loop gain. As a result, the phase noise suppression is limited and the utilization of wide linewidth laser sources would lead to a large number of cycle slips for other than short loop delays. Therefore, OPLL phase noise suppression is poor and laser linewidths are required to be less than a few megaHertz for high performance loops with practical values of loop delay. The OPLL experiment was a good example of the problems of using wide linewidth lasers and loops with a considerable delay. For the system in question, the phase noise suppression was extremely poor as the lasers had 36 MHz summed linewidth for a loop propagation delay of 15 ns, resulting in a phase error variance of around 1 rad^2 in 500 MHz measurement bandwidth.

The OIL system can offer acceptable phase noise suppression for realistic values of laser linewidth, as seen in Section III. However, the amount of power injected into the slave laser cavity (injection ratios > -40 dB) to provide low phase noise leads to limitation in the stable locking range of such systems. For example, measurements with typical DFB lasers show that the OIL unstable region, at an injection ratio of -31.4 dB, limits the useful part of the locking range to less than 1.2 GHz.

The OIPLL presented better characteristics than either of these locking techniques used separately. The tracking capability of the combined system is improved in relation to the equivalent OPLL and OIL systems, as long term fluctuations can be compensated electronically by the OPLL path while fast fluctuations can be followed by the OIL path. Theoretically, this results in better phase noise suppression in relation to the equivalent OPLL and wider stable locking range than that of an OIL system provided path mismatch is well controlled.

During the experimental investigation of the homodyne OIPLL system, it was confirmed that the OIPLL offers lower values of phase error variance (lowest value 0.006 rad^2, 500 MHz bandwidth, injection ratio -31.4 dB) when compared to that of the corresponding OPLL system (0.974 rad^2, 500 MHz bandwidth) and wider stable locking range ($>$26 GHz, injection ratio -31.4 dB) than that of the corresponding OIL system ($<$1.2 GHz). The OIPLL architecture was also extended to an heterodyne configuration, operating at 8 GHz offset and at 16 GHz offset using side frequency injection locking to a modulated master laser. The combined system offers lower values of phase error variance (0.003 rad^2, 100 MHz bandwidth) and improved stability (mean time to cycle slips of 3×10^{10} s), than are possible with wide linewidth lasers used in conventional OPLL systems, and wider stable locking range ($>$24 GHz) than a comparable OIL system ($<$2 GHz).

The OIPLL approach permits high performance loops to be realized using wide linewidth lasers, without the need for ultra wide band, short loop delay control electronics. Monolithic integration of the key components as a photonic integrated circuit would permit an elegant solution to the path matching requirement, leading to many applications in microwave and coherent optoelectronics as well as in dense wavelength division multiplex (DWDM) optical communication systems.

ACKNOWLEDGMENT

The authors would like to thank Dr. D. Wake of BT Laboratories, U.K., for the supply of DFB lasers for use in the experimental systems.

REFERENCES

[1] J. M. Kahn, "1 Gbit/s PSK homodyne transmission system using phase-locked semiconductor lasers," *IEEE Photon. Electron. Lett.*, vol. 1, pp. 340–342, Oct. 1989.
[2] L. G. Kazovsky and D. A. Atlas, "A 1320-nm experimental optical phase-locked loop: Performance investigation and PSK homodyne experiments at 140 Mb/s and 2 Gb/s," *J. Lightwave Technol.*, vol. 8, pp. 1415–1425, Sept. 1990.
[3] R. T. Ramos and A. J. Seeds, "Fast heterodyne optical phase-lock loop using double quantum well laser diodes," *Electron. Lett.*, vol. 28, no. 1, pp. 82–83, 1992.
[4] A. C. Bordonalli, B. Cai, A. J. Seeds, and P. J. Williams, "Generation of microwave signals by active mode locking in a gain bandwidth restricted laser structure," *IEEE Photon. Technol. Lett.*, vol. 8, pp. 151–153, Jan. 1996.
[5] K. R. Wendt and G. L. Fredendall, "Automatic frequency and phase control of synchronization in television receivers," *Proc. IRE*, vol. 31, pp. 7–15, 1943.
[6] M. Peter and M. W. P. Strandberg, "Phase stabilization of microwave oscillators," *Proc. IRE*, no. 43, pp. 869–873, 1955.
[7] Y. A. Bykovskii *et al.*, "Use of a Fabry–Perot resonator for the stabilization of the frequency of an injection laser," *Sov. Phys.—Semiconductors*, vol. 4, pp. 580–583, 1970.
[8] S. Yamaguchi and M. Suzuki, "Frequency stabilization of a diode laser by use of the optogalvanic effect," *Appl. Phys. Lett.*, vol. 11, pp. 597–598, 1982.
[9] U. Gliese, N. T. Nielsen, M. Bruun, E. L. Christensen, K. E. Stubkjaer, S. Lindgren, and B. Broberg, "A wideband heterodyne optical phase-

locked loop for generation of 3–18 GHz microwave carriers," *IEEE Photon. Technol. Lett.*, vol. 4, pp. 936–938, Aug. 1992.
[10] S. Kobayashi and T. Kimura, "Coherence of injection phase-locked AlGaAs semiconductor laser," *Electron. Lett.*, vol. 16, no. 7, pp. 668–670, 1980.
[11] R. Hui, A. Mecozzi, A. D'Ottavi, and P. Spanno, "Injection locking in distributed feedback semiconductor lasers," *IEEE J. Quantum Electron.*, vol. 27, pp. 1688–1695, June 1991.
[12] O. Lidoyne, P. Gallion, C. Chabran, and G. Debarge, "Locking range, phase noise and power spectrum of an injection-locked semiconductor laser," *Inst. Elec. Eng. Proc.*, vol. 137, pt. J, no. 3, pp. 147–154, 1990.
[13] A. C. Bordonalli, A. J. Seeds, and R. T. Ramos, "Low phase noise optical phase-lock loops using combined injection locking and phase locking," in *Inst. Elec. Eng. Colloquium on Microwave Opto-Electronics*, London, U.K., Dig. 1994/022, 1994, pp. 6/1–6/5.
[14] R. T. Ramos, P. Gallion, D. Erasme, A. J. Seeds, and A. C. Bordonalli, "Optical injection locking and phase-lock loop combined systems," *Opt. Lett.*, vol. 19, no. 1, pp. 4–6, 1994.
[15] A. C. Bordonalli, C. Walton, and A. J. Seeds, "High performance homodyne optical injection phase-lock loop using wide linewidth semiconductor lasers," *IEEE Photon. Technol. Lett.*, vol. 8, no. 9, pp. 1217–1219, 1996.
[16] T. G. Hodgkinson, "Phase-locked-loop analysis for pilot carrier coherent optical receivers," *Electron. Lett.*, vol. 21, no. 25/26, pp. 1202–1203, 1985.
[17] L. G. Kazovsky, "Performance analysis and linewidth requirements for optical PSK heterodyne communication systems," *J. Lightwave Technol.*, vol. LT-4, pp. 415–425, Apr. 1986.
[18] M. Ohtsu, *Highly Coherent Semiconductor Lasers*, 1st ed. Boston, MA: Artech House, 1992.
[19] F. M. Gardner, *Phaselock Techniques*, 2nd ed. New York: Wiley, 1979.
[20] G. P. Agrawal and N. K. Dutta, *Semiconductor Lasers*, 2nd ed. New York: Van Nostrand Reinhold, 1993.
[21] B. Cai, D. Wake, and A. J. Seeds, "Microwave frequency synthesis using injection locked laser comb line selection," in *Proc. LEOS Summer Topical Meetings*, Keystone, 1995, Digest no. 95TH8031, Paper WD2, pp. 13–14.
[22] O. Lidoyne, P. Gallion, and D. Erasme, "Analysis of a homodyne receiver using injection-locked semiconductor laser," *J. Lightwave Technol.*, vol. 9, pp. 659–665, May 1991.
[23] R. T. Ramos and A. J. Seeds, "Delay, linewidth and bandwidth limitations in optical phase-locked loops," *Electron. Lett.*, vol. 26, no. 6, pp. 389–391, 1990.
[24] C. Walton, A. C. Bordonalli, and A. J. Seeds, "High performance heterodyne optical injection phase-lock loop using wide linewidth semiconductor lasers," *IEEE Photon. Technol. Lett.*, vol. 10, pp. 427–429, Mar. 1998.

A. C. Bordonalli, photograph and biography not available at the time of publication.

C. Walton, photograph and biography not available at the time of publication.

Alwyn J. Seeds (M'81–SM'92–F'97) received the Ph.D. degree from the University of London, London, U.K., in 1980 for work on the optical control of IMPATT oscillators.

From 1980 to 1983, he was a Staff Member at Lincoln Laboratory, Massachusetts Institute of Technology, Lexington, where he worked on GaAs monolithic millimeter-wave integrated circuits for use in phased-array radar. In 1983, he returned to England to take-up a lectureship in telecommunications at Queen Mary College, University of London, and in 1986, he moved to University College London, U.K., where he is now Professor of Opto-electronics and Head of the Opto-electronics and Optical Networks Group. He has published over 150 papers on microwave and optoelectronic devices and their systems applications and is the presenter of the video "Microwave Opto-electronics" in the IEEE Emerging Technologies series. His current research interests include microwave bandwidth tunable lasers, optical control of microwave devices, mode-locked lasers, optical phase-lock loops, optical frequency synthesis, dense WDM networks, optical soliton transmission, and the application of optical techniques to microwave systems.

Dr. Seeds is Vice-Chairman of Commission D (Electronics and Photonics) of the International Union for Radio Science (URSI), a Chairman of the technical committee on Lightwave Technology of the IEEE Microwave Theory and Techniques Society. He has served on the program committees for many international conferences, and is General Chair for the forthcoming IEEE MTT/LEOS International Topical Meeting on Microwave Photonics (MWP 2000) in Oxford, U.K.